

CHARMM Force-Fields with Modified Polyphosphate Parameters Allow Stable Simulation of the ATP-Bound Structure of Ca^{2+} -ATPase

Yasuaki Komuro,^{†,‡,§} Suyong Re,[‡] Chigusa Kobayashi,[§] Eiro Muneyuki,[†] and Yuji Sugita^{*,‡,§,||,⊥}

[†]Graduate School of Science and Engineering, Chuo University, 1-13-27, Kasuga, Bunkyo-ku, Tokyo 112-8551, Japan

[‡]RIKEN Theoretical Molecular Science Laboratory, 2-1, Hirosawa, Wako-shi, Saitama 351-0198, Japan

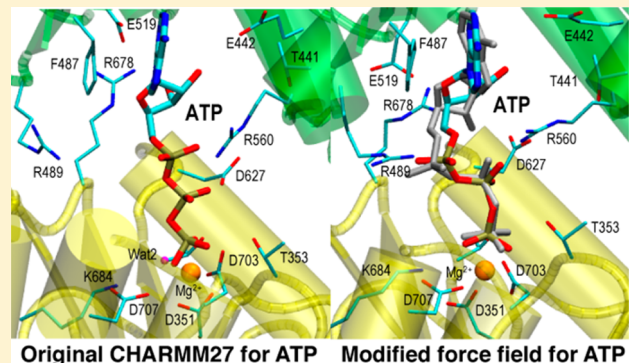
[§]RIKEN Advanced Institute for Computational Science, International Medical Device Alliance (IMDA) 6F, 1-6-5 minatojima-minamimachi, Chuo-ku, Kobe, Hyogo 650-0047, Japan

^{||}RIKEN Quantitative Biology Center, International Medical Device Alliance (IMDA) 6F, 1-6-5 minatojima-minamimachi, Chuo-ku, Kobe, Hyogo 650-0047, Japan

[⊥]RIKEN iTHES, 2-1, Hirosawa, Wako-shi, Saitama 351-0198, Japan

Supporting Information

ABSTRACT: Adenosine triphosphate (ATP) is an indispensable energy source in cells. In a wide variety of biological phenomena like glycolysis, muscle contraction/relaxation, and active ion transport, chemical energy released from ATP hydrolysis is converted to mechanical forces to bring about large-scale conformational changes in proteins. Investigation of structure–function relationships in these proteins by molecular dynamics (MD) simulations requires modeling of ATP in solution and ATP bound to proteins with accurate force-field parameters. In this study, we derived new force-field parameters for the triphosphate moiety of ATP based on the high-precision quantum calculations of methyl triphosphate. We tested our new parameters on membrane-embedded sarcoplasmic reticulum Ca^{2+} -ATPase and four soluble proteins. The ATP-bound structure of Ca^{2+} -ATPase remains stable during MD simulations, contrary to the outcome in shorter simulations using original parameters. Similar results were obtained with the four ATP-bound soluble proteins. The new force-field parameters were also tested by investigating the range of conformations sampled during replica-exchange MD simulations of ATP in explicit water. Modified parameters allowed a much wider range of conformational sampling compared with the bias toward extended forms with original parameters. A diverse range of structures agrees with the broad distribution of ATP conformations in proteins deposited in the Protein Data Bank. These simulations suggest that the modified parameters will be useful in studies of ATP in solution and of the many ATP-utilizing proteins.



contrary to the outcome in shorter simulations using original parameters. Similar results were obtained with the four ATP-bound soluble proteins. The new force-field parameters were also tested by investigating the range of conformations sampled during replica-exchange MD simulations of ATP in explicit water. Modified parameters allowed a much wider range of conformational sampling compared with the bias toward extended forms with original parameters. A diverse range of structures agrees with the broad distribution of ATP conformations in proteins deposited in the Protein Data Bank. These simulations suggest that the modified parameters will be useful in studies of ATP in solution and of the many ATP-utilizing proteins.

INTRODUCTION

Proteins in cells function as molecular machines under the influence of significant disturbance from thermal noise. Motor proteins and membrane transporting proteins commonly utilize adenosine triphosphate (ATP) as a substrate to carry out their functions in such conditions. They convert chemical energy released from ATP hydrolysis to mechanical forces and undergo large-scale conformational changes to effect their specific function. Molecular mechanisms underlying the energy conversion have been investigated extensively both experimentally and theoretically. X-ray crystal structures of ATP-bound proteins are, in particular, useful for understanding function at an atomic level. Approximately 1300 structures of ATP-bound proteins are in the Protein Data Bank (<http://www.pdb.org/>).

Ca^{2+} -ATPase of skeletal muscle sarcoplasmic reticulum (SERCA1a) is, structurally and functionally, one of the best-

studied proteins utilizing ATP. The ATPase is an integral membrane protein that transports two Ca^{2+} from the cytoplasm into the lumen of the sarcoplasmic reticulum (SR) against a 10⁴-fold concentration gradient.¹ According to classical E1/E2 theory, the transmembrane Ca^{2+} -binding sites have high affinity for Ca^{2+} and face the cytoplasm in the E1 state, whereas they have low affinity and face the lumen of the SR in the E2 state.^{2–4} Biochemical studies established that ATP binds on the cytoplasmic side, and X-ray crystallography placed the binding site at P and N domains and provided atomic coordinates of the bound ATP conformation.^{5,6} There are still unsolved questions concerning how ATP contributes to ATPase function.^{7–12} How is the chemical energy from ATP hydrolysis converted into mechanical forces that transfer bound Ca^{2+} to the lumen,

Received: May 13, 2014

considering that the transmembrane binding sites of Ca^{2+} are about 50 Å away from the ATP binding site? Answers lie not only in the structures but also in the dynamics.

Molecular dynamics (MD) simulation is an important research tool used to investigate protein dynamics in solvent or in biological membranes. Previous studies of MD simulations of Ca^{2+} -ATPase mostly focused on the Ca^{2+} -binding sites or structural transitions between different intermediate states. Ca^{2+} -binding site simulations with all-atom models have investigated the stability of the bound Ca^{2+} ,¹³ the ion transport pathway,¹⁴ and the protonation states of the residues in the Ca^{2+} -binding sites.^{15–17} Likewise, all-atom models have explored the large structural transition between E1·2 Ca^{2+} and E1·ATP states,¹⁸ whereas coarse-grained representations have illuminated transitions between the E1·2 Ca^{2+} and E2 states^{19,20} and between E1·2 Ca^{2+} and E1·ATP.²¹ Normal mode analysis has analyzed motions of the three cytoplasmic domains of the Ca^{2+} -ATPase.^{22–24} In this study, the conformation of ATP bound to Ca^{2+} -ATPase is studied using an all-atom model.

ATP consists of adenine, ribose, and a string of three phosphates. ATP binds strongly to the P- and N-domains of Ca^{2+} -ATPase due largely to strong electrostatic interactions between phosphates and protein. Standard force-field parameters of ATP have worked reasonably well in simulations performed on many ATP-bound proteins but, as shown here, are inadequate for representation of ATP-bound Ca^{2+} -ATPase.^{25–39} Accordingly, we modified the force-field parameters of the triphosphate moiety based on high-precision quantum chemical calculations and tested the new parameters in MD simulations of Ca^{2+} -ATPase as well as other ATP-bound proteins. In addition, we compared the accessible conformational space of an ATP molecule in water using modified and original parameters in replica-exchange MD (REMD) simulations.⁴⁰ Finally, we discuss the general applicability of the currently developed force-field parameters of ATP for modeling many other ATP-utilizing proteins.

MATERIAL AND COMPUTATIONAL METHODS

Changing Polyphosphate Parameters in the CHARMM Force Field. The original CHARMM27 force-field parameters for polyphosphates (C27(ATP))⁴¹ were reparameterized by employing a standard CHARMM procedure. We used methyl triphosphate (MTP; Figure 1a) as a model compound instead of the methyl diphosphate (MDP; Figure 1b) used in original CHARMM27 force-field parameterization.⁴¹ High-precision *ab initio* data were obtained at the MP2/6-31+G* level of quantum chemical theory. All quantum chemical calculations were performed using Gaussian 09.⁴²

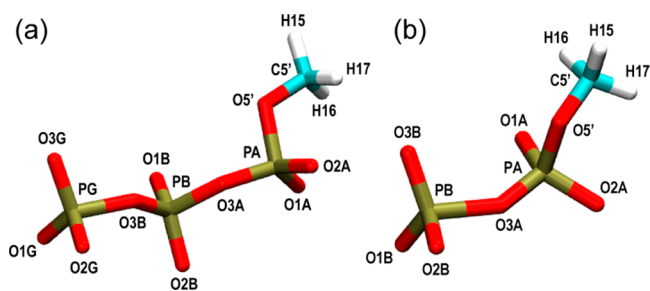


Figure 1. Structures of model compounds (a) methyl triphosphate (MTP), (b) methyl diphosphate (MDP).

We modified only bond angle and dihedral angle parameters, not nonbonded parameters, in order to preserve consistency with existing force-fields. Force constants (K_θ) and equilibrium angle values (θ_0) of MTP were slightly modified and the Urey–Bradley (UB) terms were removed from the P–O–P angles (Table 1). Original CHARMM force fields used UB terms of

Table 1. Bond Angle Parameters for Polyphosphate Determined in This Study (mod-C27(ATP))^a

type of bond angles	K_θ	θ_0	K_{UB}	s_0
P2–ON2–P	25.37 (15.0)	150.0 (140.0)	0 (−40.0)	0 (2.80)
P2–ON2–P2	25.37 (15.0)	150.0 (140.0)	0 (−40.0)	0 (2.80)
ON2–P–ON2	90.0 (80.0)	102.6 (104.3)		
ON2–P2–ON2	90.0 (80.0)	102.6 (104.3)		
ON2–P2–ON3	100.0 (88.9)	108.23 (111.6)		

^aThe original CHARMM27 force-field parameters (C27(ATP)) are also shown in parentheses.

P–O–P with negative force constants to reproduce vibrational frequencies obtained with *ab initio* calculations. Practical difficulties prevented adherence to accurate reproduction of both equilibrium geometry and vibrational frequencies, and we focused primarily on geometry. Force constants (K_ϕ), multiplicity (n), and phase (δ) of dihedral angle terms in MTP were reparameterized to reproduce potential energy profiles at the MP2/6-31+G* level. The energy profiles were scanned in 15° increments in both forward and backward directions. The parameters were determined by fitting the empirical energy profile to the entire range of the *ab initio* profile.⁴³ Note that the dihedral angle of C5'–O5'–PA–O3A was fixed at 180° during geometry optimization and dihedral angle scanning.⁴⁴ This constraint avoids formation of an intramolecular hydrogen bond between the phosphate and the methyl groups. In physiological conditions, solvation and counterions would prevent such a hydrogen bond. Note that the modified force-field parameters can be used for polyphosphate molecules such as nucleoside triphosphates (ATP, GTP, CTP, and UTP) and diphosphates (ADP, GDP, CDP, and UDP). Our modified parameters include the bond angle term, ON2–P–ON2, which is also used for the phosphodiester bond in DNA or RNA. In the original CHARMM force field, ATP/ADP and DNA/RNA share the same parameter for this bond angle.^{41,45,46} However, in this study, we do not intend to use the same modified parameters in DNA or RNA simulations. The topology and parameter files of the modified force field, mod-C27(ATP), are appended to Supporting Information.

MD Simulations of ATP-Bound State of Ca^{2+} -ATPase and Other Proteins. The initial configuration of Ca^{2+} -ATPase in MD simulations was constructed using the X-ray crystal structure of the E1·ATP state (PDB entry: 1VFP).⁵ AMPPCP and Ca^{2+} in the crystal structure were replaced with ATP and Mg^{2+} , respectively. We inserted a K^+ into a cavity in the P-domain, since K^+ is observed here in the X-ray crystal structure of E1·2 Ca^{2+} .⁴⁷ Glu908 in the Ca^{2+} -binding sites was protonated according to its predicted pK_a value.¹⁵ Hydrogen atoms were added to the crystal structure using the VMD 1.9.1 tool set.⁴⁸ Cavities inside the protein were filled with water molecules using DOWSER.⁴⁹ This structure was embedded in a pre-

equilibrated dioleoylphosphatidylcholine (DOPC) lipid bilayer.^{50–52} The orientation of the protein with respect to the bilayer normal is the same as that used in our previous study on E1·2Ca²⁺.^{13,15} Finally, the system was solvated and neutralized with 150 mM KCl (Figure 2).

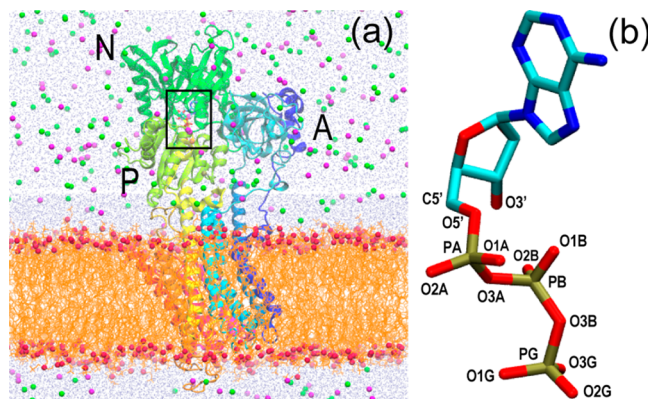


Figure 2. Initial structural model of the MD simulation for Ca²⁺-ATPase. (a) Overview of a unit cell. The crystal structure of ATP-bound form of Ca²⁺-ATPase in DOPC membrane with explicit solvent molecules. A, N, and P indicate the actuator, the nucleotide-binding, and the phosphorylation domains, respectively. The colors are blue, N-terminus domain; yellow, middle domain; red, C-terminus domain; orange, lipid bilayer; green sphere, K⁺; magenta sphere, Cl⁻. (b) Enlarged view of the structure of ATP (which replaces AMPPCP) in the crystal structure of Ca²⁺-ATPase.

We carried out all-atom MD simulations of the Ca²⁺-ATPase in the E1·ATP state with explicit solvent and a DOPC lipid bilayer. CHARMM27 force fields with φ , ψ cross-term map correlation (CMAP) were used for the protein.^{53,54} CHARMM36 was used for lipid molecules.⁵⁵ The TIP3P model⁵⁶ of water was employed. Ion parameters of Villa et al.⁵⁷ and Åqvist⁵⁸ were used for Mg²⁺ and Ca²⁺, respectively. We used the original CHARMM27 parameters (C27(ATP))⁴¹ and our modified version (mod-C27(ATP)) for ATP in different MD simulations. All bonds involving hydrogen atoms in the protein were constrained using SHAKE,⁵⁹ and water molecules were treated as rigid bodies using SETTLE.⁶⁰ The equation of motion was integrated with a time step of 2 fs based on a velocity-verlet scheme. Long-range electrostatic interactions were calculated using particle-mesh Ewald summation.⁶¹ Lennard-Jones interactions were truncated at a distance of 12 Å (with a switching function being effective at 10 Å). Temperature (310 K) and pressure (1 atm) were held constant by using Langevin dynamics with a damping coefficient of 5 ps⁻¹ and the Langevin piston Nosé–Hoover method,^{62,63} respectively. All simulations were performed using the NAMD program package.⁶⁴

The simulation system was minimized using the conjugate gradient method in two consecutive steps: heavy atoms of protein, lipids, and ATP as well as ions were held fixed in the first 1000 steps, and harmonic restraint potentials were applied for the next 9000 steps (10.0 kcal/mol·Å² for the heavy atoms of proteins, lipids, and ATP, and 1.0 kcal/mol·Å² for ions). Next, the system was equilibrated in the NVT ensemble for 200 ps with the same restraint potentials. Further equilibration was performed in the NPT ensemble for 400 ps with reduced restraints (1.0 kcal/mol·Å² for the heavy atoms of protein, ATP and ions and 10.0 kcal/mol·Å² for the heavy atoms of lipids

only in the z-axis direction). The last 400 ps of equilibration was performed by gradually reducing the restraints on heavy atoms of the protein and ATP from 1.0 kcal/mol·Å² to zero. We performed a 20 ns production run in the NPT ensemble without restraints.

To validate the modified polyphosphate parameters, we also performed MD simulations of four other ATP-bound proteins. We selected four proteins for which X-ray crystal structures at high resolution (less than 1.5 Å) are available. They are histidine permease (PDB: 1b0u), RNA editing ligase MPS2 (PDB entry: 1xdn), phosphoribosylamidoimidazole-succinocarboxamide synthase (PDB entry: 1obd), and α -skeletal muscle actin (PDB entry: 2fxu). Each system was equilibrated in a similar manner to Ca²⁺-ATPase. We performed a 5 ns production run for each protein. Summary of the simulation systems are given in Table S1.

REMD Simulations of ATP in Water. Equilibrium conformations of ATP with original (C27(ATP)) or modified (mod-C27(ATP)) parameters were investigated by performing REMD simulations of ATP in explicit solvent. The initial conformation of ATP was taken from the equilibrated structure of E1·ATP in MD simulations. ATP was then solvated in 150 mM KCl solution. We used in-house software REIN (Replica-Exchange Interface)⁶⁵ for the REMD simulations. NAMD was used for the MD simulation of each replica. We employed 24 replicas in the NVT ensemble at temperatures of 300–400 K, which were generated by the REMD temperature simulator.⁶⁶ Replica exchanges were performed every 1000 steps. Each replica was simulated for 200 ps without exchange to equilibrate the system. Simulations were carried out for 480 ns in total (= 20 ns × 24 replicas). Only the trajectory at 300 K was used in our analyses. A summary of the system is given in Table S1.

RESULTS AND DISCUSSION

In the E1·ATP state of Ca²⁺-ATPase, ATP binds near the hinge between the N and P domains, thereby constraining them into a compact headpiece.^{7,10,11,67} The polyphosphate moiety of ATP in the crystal structure adopts a zigzag configuration (Figure 2b). In this configuration, the oxygen atoms of the β -phosphate face the ribose (Figure 3a). Phe487 stabilizes the adenine ring of ATP by a stacking interaction.^{47,68,69} Arg489

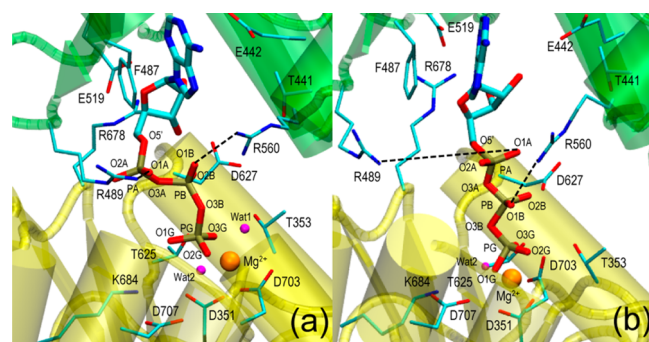


Figure 3. Enlarged views of the ATP-binding site in X-ray crystal structure (a) and a snapshot after 5 ns MD simulation using C27(ATP) (b). AMPPCP in the crystal structure was replaced by ATP. The colors are green, N-domain; yellow, P-domain; orange sphere, Mg²⁺; red sphere, water. Dotted lines show two salt bridges: one between ATP (α -phosphate) and Arg489 side chain and another between ATP (β -phosphate) and Arg560 side chain.

and Arg560 interact with the α -phosphate and the β -phosphate, respectively.^{5,6,70–72} Many polar groups (a carboxyl group of Asp351, hydroxyl groups of Thr353 and Thr625, amide groups of Thr353 and Gly626, a carbonyl group of Thr353) and Mg²⁺ stabilize the γ -phosphate.⁵ Mutation of any of these residues alters ATPase function.^{73–75} Arg560 in the N-domain orients the phosphate chain of ATP to facilitate salt-bridge (SB) formation with Asp627 in the P domain, thereby consolidating interaction of N and P domains.^{76–78}

MD Simulation of ATP-Bound Form of Ca²⁺-ATPase Using Original C27(ATP) Parameters. A comparison of the ATP-binding site in Ca²⁺-ATPase in the final snapshot of the 5 ns-MD simulation using C27(ATP) with that in the X-ray crystal structure indicates that the triphosphate structure changes very quickly from zigzag to extended form (Figure 3b). Figure 4a shows the time courses of two SB distances: one

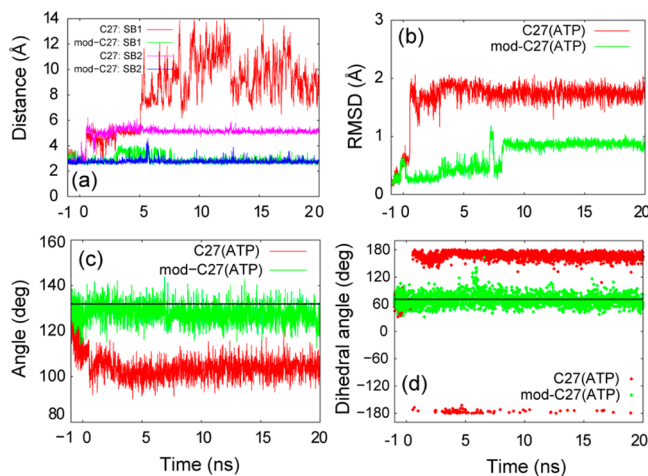


Figure 4. Time course of the selected structural parameters in 20 ns MD simulations using C27(ATP) or mod-C27(ATP). (a) Salt bridge (SB) distances: SB1 between α -phosphate and Arg489 (red line for C27(ATP) and green one for mod-C27(ATP)) and SB2 between β -phosphate and Arg560 (magenta for C27(ATP) and blue for mod-C27(ATP)). (b) RMSD of triphosphate moiety, (c) PA–O3A–PB bond angle, (d) OS'–PA–O3A–PB dihedral angle. The black lines in c and d show the corresponding distances observed in the X-ray structure.

between the α -phosphate and Arg489 side chain and the other between the β -phosphate and Arg560 side chain. Biochemical experiments with Ca²⁺-ATPase and other P-type ATPases, including Na⁺,K⁺-ATPase, indicate that these SBs do stabilize the ATP–protein complex.^{76–78} However, both were immediately broken in the simulation due to drastic decreases in P–O–P angles linking the α -, β -, and γ -phosphates (Figure 4c). The average values of PA–O3A–PB and PB–O3B–PG angles in the simulation are 104° and 111°, respectively. They are much smaller (by 28° and 12°, respectively) than those in the X-ray crystal structure (Table 4). Note that O3B in the PB–O3B–PG angle corresponds to the carbon atom of AMPPCP that is used as an analogue of ATP to produce the crystals. Due to the decreases in the P–O–P bond angles, the α -, β -, and γ -phosphate oxygen atoms approach one another, and the dihedral angles change to minimize repulsive electrostatic interactions (Figure 4b and d).

MD Simulation Using mod-C27(ATP) Parameters. Next, we performed another MD simulation of the same system, changing only ATP force-field parameters (mod-

C27(ATP)). The final dihedral parameter sets for polyphosphate are shown in Table 2. The mod-C27(ATP) parameters

Table 2. Dihedral Angle Parameters for Polyphosphate Determined in This Study (mod-C27(ATP))^a

dihedral type	K_ϕ	n	δ
P2–ON2–P–ON2	0.4485	1	0
	(0.03)	(2)	(0)
	(0.03)	(3)	(0)
P–ON2–P2–ON2	0.4485	1	0
	(0.03)	(2)	(0)
	(0.03)	(3)	(0)
P2–ON2–P2–ON2	0.4485	1	0
	(0.03)	(2)	(0)
	(0.03)	(3)	(0)
P–ON2–P2–ON3	−0.7090	2	0
	(0.10)	(2)	(0)
	(0.03)	(3)	(0)

^aThe original CHARMM27 force-field parameters (C27(ATP)) are also shown in parentheses.

better reproduce the potential energy profiles along the selected dihedral angles calculated using high level *ab initio* method (MP2/aug-cc-pVTZ//MP2/6-31+G*) compared with the original parameters, C27(ATP) (Figure S1). The root-mean-square errors (RMSEs) of the empirical potential energies with respect to the *ab initio* energies for the seven dihedral angles are listed in Table 3. The modified force-field parameters had in

Table 3. Root Mean Square Error (RMSE) of the Empirical Potential Energy Surfaces (C27(ATP) and mod-C27(ATP)) along the Selected Dihedral Angles with Respect to the Corresponding *ab Initio* Potential at the MP2/6-31+G* Level

RMSE (kcal/mol)		
dihedral angle	C27(ATP)	mod-C27(ATP)
C5'–OS'–PA–O3A	2.43	1.22
O5'–PA–O3A–PB	4.41	2.12
PA–O3A–PB–O3B	6.93	3.30
O3A–PB–O3B–PG	0.48	1.35
PB–O3B–PG–O1G	0.11	0.24
C5'–OS'–PA–O1A	2.48	1.30
PA–O3A–PB–O1B	6.94	2.72
average	3.40	1.75

general better agreement with *ab initio* results compared with the originals. The average RMSE value for mod-C27(ATP) is roughly half of that for C27(ATP). Figure 4b shows the root-mean-square deviation (RMSD) of the triphosphate with respect to the initial structure. In contrast to the previous simulation, the structure of ATP remains stable as per the X-ray crystal structure, taking a zigzag form. The time series of P–O–P angles fluctuate around those in the crystal structure (Figure 4c). The average values of PA–O3A–PB and PB–O3B–PG angles in the MD simulation are 128° and 133°, respectively, which are close to those in the X-ray crystal structure (Table 4). The average values of the OS'–PA–O3A–PB dihedral angle in the MD simulation is 70.2° which is almost the same as that in the X-ray crystal structure (70.9°, Table 4). Clearly, the agreement is much better than that obtained with original C27(ATP) parameters. Figure 4c and d show the time course

Table 4. Averaged Bond and Dihedral Angles (in Degrees) (PA–O3A–PB, PB–O3B–PG and OS'–PA–O3A–PB) of the ATP Bonded to Ca²⁺-ATPase Obtained from 20 ns-MD Simulations Using C27(ATP) and mod-C27(ATP)^a

angles	MD simulations		X-ray structure
	C27(ATP)	mod-C27(ATP)	
bond angles PA–O3A–PB	104 (4.4)	128 (4.5)	132
bond angles PB–O3B–PG	111 (5.9)	133 (4.8)	123
dihedral angle OS'–PA–O3A–PB	164 (19)	70.2 (13)	70.9

^aThe numbers in parentheses are standard deviations. The corresponding values from the X-ray crystal structure are also shown for comparison.

of the PA–O3A–PB angle and the OS'–PA–O3A–PB dihedral angle, respectively. Both values stay close to those of the X-ray structure during 20 ns of MD simulation. Two important SBs are maintained in the 20 ns MD simulation (Figure 4a). PA, PB, and PG atoms of ATP in each frame of the trajectory remained superimposed. In Table 5, the average

Table 5. Average Distances (in Å) of Selected Interactions in the ATP Binding Site Obtained from 20 ns-MD Simulations

type of interactions	MD simulations		X-ray structure
	C27(ATP)	mod-C27(ATP)	
ATP (O3')–R678 (NH2)	4.93	2.96	3.10
ATP (O1G)–G626 (N)	4.15	2.95	2.82
ATP (O3G)–T353 (OG1)	4.09	2.59	2.57
D627 (OD1)–R678 (NH2)	8.80	4.74	3.86
R560 (NH1)–D627 (OD2)	5.31	2.74	2.83

distance deviations of the structures in MD simulation from the crystal structure are listed for other SBs as well as hydrogen bonds in the ATP binding site. All of these interactions are important for N–P interdomain interaction induced by ATP binding. The average deviation from the crystal structure is reduced from 2.42 Å for C27(ATP) to 0.16 Å for mod-C27(ATP). The ATP binding mode in the MD simulation is in good agreement with that in the X-ray crystal structure due to preservation of internal and intermolecular interactions. (Figure 5).

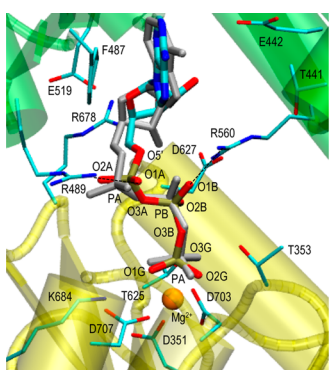


Figure 5. A snapshot of ATP-binding site after 20 ns-MD simulation using mod-C27(ATP). The X-ray crystal structure of ATP bounded to Ca²⁺-ATPase (gray) is shown for comparison.

The interaction with metal ions, such as Mg²⁺, is important in most biological context. Various models have been developed for better describing metal ions in the classical MD simulations.^{57,58,79–87} We performed 20 ns MD simulation of the same system employing one of the decent models for Mg²⁺ and Ca²⁺ developed by Merz and his colleagues.⁸⁶ Time course of the selected structural parameters from the simulations and a snapshot of ATP-binding site after 20 ns are shown in Figures S2 and S3, respectively. We found that the binding mode of the triphosphate moiety in ATP was retained as the X-ray structure, although the ribose and adenine ring were slightly rotated. Trends of the time courses of the structural parameters were similar to those with ion parameters by Villa et al.⁵⁷ and Åqvist⁵⁸ for Mg²⁺ and Ca²⁺, respectively (Figures 4 and 5). The results confirm, at least, the compatibility with the decent models for metal ions to better describe the ion–ATP interactions.

We also tested mod-C27(ATP) parameters in MD simulations of four other ATP-bound proteins in solution. For this purpose, we selected four proteins for which high-resolution (less than 1.5 Å) crystal structures are available. They are histidine permease (PDB: 1b0u), RNA editing ligase MP52 (PDB entry: 1xdn), phosphoribosylamidoimidazole-succinocarboxamide synthase (PDB entry: 1obd), and α -skeletal muscle actin (PDB entry: 2fxu). The global structures and close-up views of their ATP-binding sites are shown in Figure 6. Figure S4 shows RMSD of the triphosphate moiety in ATP with respect to the initial structure. Except for the simulation of RNA editing ligase MP52, time-courses for the RMSD are similar between C27(ATP) and mod-C27(ATP). But, in all four of the cases, the simulations based on mod-C27(ATP) reproduce the triphosphate structure in ATP better than do those using original parameters.

REMD Simulations of ATP in Solution. The MD simulations of the ATP-bound proteins including Ca²⁺-ATPase suggest that the original C27(ATP) parameters have shortcomings, at least in some systems. To better understand this, we performed replica-exchange molecular dynamics (REMD) simulations of an ATP molecule in solution and examined the conformational spaces of the triphosphate moiety at room temperature in solution comparing outcomes with C27(ATP) parameters or mod-C27(ATP). Random walks in temperature and potential energy spaces in the REMD simulations are shown in Figure S5. The average acceptance ratios were 51.7% and 50.7% for C27(ATP) and mod-C27(ATP) parameters, respectively. This suggests that the replica-exchange method works well in both simulations.

Potential of mean forces (PMFs) at 300 K along the two angles, PA–O3A–PB (ang1) and PB–O3B–PG (ang2), are shown in Figures 7a (C27(ATP)) and b (mod-C27(ATP)). For comparison, corresponding angles from 59 crystal structures of ATP-bound proteins are also plotted. The minimum free-energy region (dark blue in the figure) in the simulation with C27(ATP) is located around (ang1, ang2) = (100°, 120°), whereas that with mod-C27(ATP) is shifted to (ang1, ang2) = (120°, 130°). These differences are similar to those in the MD simulations of Ca²⁺-ATPase. The distributions of the angles in the simulation with mod-C27(ATP) overlap much better with those in the X-ray crystal structures. The corresponding minimum of the triphosphate moiety in the E1-ATP state of Ca²⁺-ATPase is located at (ang1, ang2) = (128°, 127°).

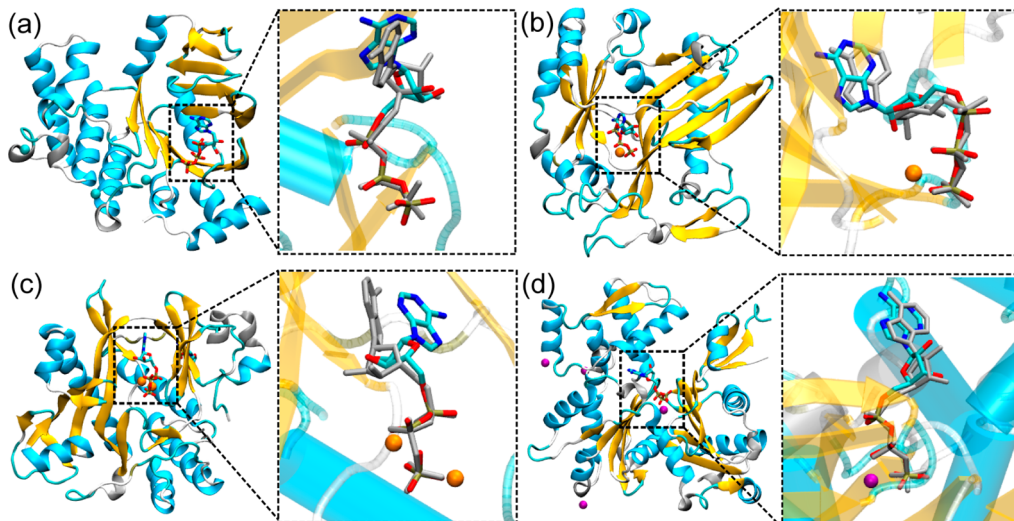


Figure 6. High resolution (less than 1.5 Å) X-ray crystal structures of ATP-bound proteins: (a) Histidine permease (PDB: 1b0u), (b) RNA editing ligase MPS2 (PDB entry: 1xdn), (c) phosphoribosylamidoimidazole-succinocarboxamide synthase (PDB entry: 1obd), and (d) α -skeletal muscle actin (PDB entry: 2fxu). ATP structures from 5 ns-MD simulations of the corresponding proteins using mod-C27(ATP) are shown in a gray color for comparison. Mg^{2+} and Ca^{2+} are shown as orange and purple spheres, respectively.

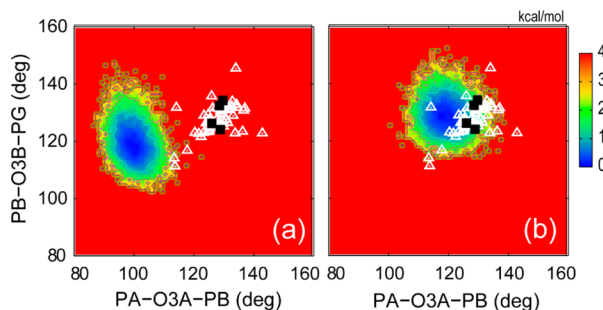


Figure 7. PMF landscapes along the PA–O3A–PB (ang1) and PB–O3B–PG (ang2) bond angles of ATP from the trajectory at 300 K in the REMD simulations using C27(ATP) (a) and mod-C27(ATP) (b). The corresponding values from 59 X-ray crystal structures of ATP-bound proteins are mapped on the surface: black squares, resolution better than 1.5 Å (4 structures); white triangle, resolution better than 2.0 Å (55 structures).

We examine PMFs along the two dihedral angles, O5'–PA–O3A–PB (**dih1**) and PA–O3A–PB–O3B (**dih2**), as reaction coordinates in Figure 8. The difference of PMFs was also calculated every 5 ns of the simulation, and convergence was seen after 5 ns as shown in Figure S6. The PMFs based on C27(ATP) parameters show a single energy minimum around (**dih1**, **dih2**) = (180°, 180°) (Figure 8a), whereas those based on mod-C27(ATP) have a much wider distribution along the **dih2** angle at 300 K (Figure 8b). If we divide the minimum energy region along the **dih2** angle in Figure 8 into four regions (I–IV; see Table 6), the REMD simulation using C27(ATP) samples regions II and III only, whereas that with mod-C27(ATP) covers structures in not only regions II and III but also regions I and IV. The minimum for the triphosphate moiety in the E1·ATP state of Ca^{2+} -ATPase is located at (**dih1**, **dih2**) = (70.9°, 95.5°), outside the four regions. These two angles belong to α - and β -phosphates that form salt bridges with Arg489 and Arg560, respectively, and have angular

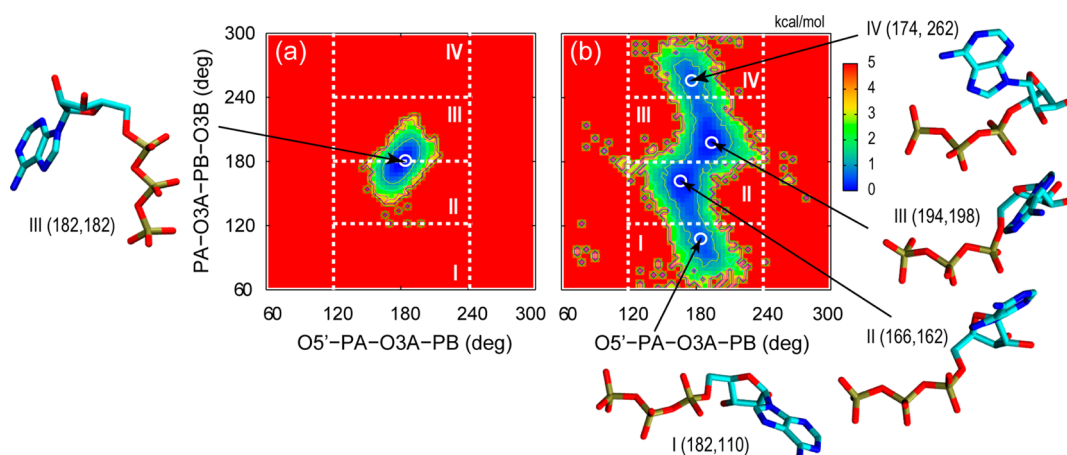


Figure 8. PMF landscapes along the O5'–PA–O3A–PB (**dih1**) and PA–O3A–PB–O3B (**dih2**) dihedral angles from the trajectory at 300 K in the REMD simulations using C27(ATP) (a) and mod-C27(ATP) (b). The dashed lines indicate the separation of the angle space used for the conformational analysis: I, $60^\circ \leq \text{dih2} < 120^\circ$; II, $120^\circ \leq \text{dih2} < 180^\circ$; III, $180^\circ \leq \text{dih2} < 240^\circ$; IV, $240^\circ \leq \text{dih2} < 300^\circ$. The representative conformation in each area is shown with the dihedral angles' values (**dih1**, **dih2**) in degrees.

Table 6. Relative Population of ATP Conformers in Regions I–IV Obtained from the REMD Simulations of ATP in Solution Using C27(ATP) and mod-C27(ATP)^a

	C27(ATP)	mod-C27(ATP)
region I	0.0	14.8 (0.4)
region II	49.8	34.5 (0.1)
region III	50.2	36.9 (0.0)
region IV	0.0	13.3 (0.4)

^aThe relative free-energy (in kcal/mol) of the representative conformer (Figure 8) in each section is shown in parentheses.

preferences different from those in water. In both parameter sets, most (dominant) structures are found in regions II and III.

If we introduce a third dihedral angle, O3A–PB–O3B–PG (**dih3**) and define the all-trans (extended) conformation as $150^\circ \leq (\text{dih1}, \text{dih2}, \text{dih3}) \leq 210^\circ$, the relative population of species with the all-trans conformation is 76.4% and 31.2% in REMD simulations using C27(ATP) and mod-C27(ATP), respectively. All other structures can be considered to be zigzag forms like the ATP bound in Ca^{2+} -ATPase. Interestingly, **dih1** and **dih2** from the 59 high-resolution crystal structures of ATP-bound proteins (resolution better than 2.0 Å) sample much wider conformational space than that suggested from the calculated PMFs of the triphosphate moiety of ATP in solution (Figures S7a and S7b). In the very high-resolution crystal structures (resolution better than 1.5 Å), two out of four fall outside of the major distribution of conformations observed in free ATP. One is RNA editing ligase MP52 (Figure 6b; 274° , 174°), and the other is phosphoribosylamidoimidazole-succinocarboxamide synthase (Figure 6c; 86.6° , 123°). Triphosphate moieties bound to proteins seem more distortable than those in solution, due to their interaction with surrounding amino-acid residues of the proteins. **dih1**–**dih2** distribution maps for the simulations of Ca^{2+} -ATPase as well as additional four ATP-binding proteins using C27(ATP) and mod-C27(ATP) are shown in Figure S7c and d. In conclusion, the intrinsic flexibility of the triphosphate moiety of ATP, both in solution and bound to proteins, is much better represented in simulations with mod-C27(ATP) parameters which allow for a wider range of conformational sampling, not only of extended forms but also of other structures such as the zigzag conformation found in Ca^{2+} -ATPase.

Comparison between Original and Modified ATP Parameters. We now summarize the differences in parametrization between the original (C27(ATP)) and our new (mod-C27(ATP)) ones for the triphosphate moiety of ATP. A major difference is the use of the model compound MDP in the original work and MTP in this study. Since MTP contains three phosphate groups, its chemical properties are much closer to those of ATP. A second difference is the level of *ab initio* quantum chemical calculations for obtaining reference energy data. Originally, the HF/6-31+G* level of theory was used, whereas we adopted the MP2/6-31+G* level, which takes electron correlation effect into account. In general, the electron correlation effect lowers energy barriers along the dihedral angles. This is most easily seen in the sampling of a much wider conformational space with the modified parameters (Figure 8). A third difference exists in the UB force constants of the P2–ON2–P and P2–ON2–P2 angles. Negative force constants were originally introduced in order to reproduce *ab initio* vibrational frequencies. The vibrational frequency of the P–O–P angle deformation in C27(ATP), calculated using the

MOLVIB facility in CHARMM,⁸⁸ is 95.5 cm^{-1} , which agrees with the *ab initio* calculation (86.8 cm^{-1} with HF/6-31+G*).⁴¹ Omitting the UB terms slightly worsens the agreement (86.6 cm^{-1} vs 128.6 cm^{-1} with MP2/6-31+G* for MDP) but gives a better description of ATP structures bound to proteins.

In aiming to reproduce different physical and chemical properties of molecules, classical force-field parameters comprise several different terms. There seems to be intrinsic difficulty in reproducing all the properties with existing force-field parameters, and different applications may need different adjustments. The faithful reproduction of equilibrium structures of the triphosphate moiety in water and of protein-bound structures may be of primary importance for biological functional studies. Our modified parameters are beneficial in this regard and could prove useful in many other applications.

CONCLUSIONS

In this study, we reparameterized the force-field parameters of the triphosphate moiety in ATP based on high-precision *ab initio* data for methyl triphosphate as a model compound. The UB term was omitted in reproducing vibrational frequencies. The modified parameters were tested by performing MD simulations of ATP-bound proteins using original and modified parameters. Further evaluation was done by performing replica-exchange molecular dynamics simulations of ATP in water. The modified parameters out-performed the originals by several criteria, more accurately reproducing ATP conformations in the protein-bound state and portraying a much wider range of conformations in water. Neglecting the UB term had a minor effect. Our modified force fields for polyphosphate could be advantageously used in molecular dynamics simulations of a wide range of nucleotide (ATP/GTP)-driven enzymatic systems.

ASSOCIATED CONTENT

Supporting Information

Summary of system preparation, model compound information, energy profiles of dihedral angles of MTP, time course of the selected structural parameter and a snapshot of ATP-binding site in 20 ns MD simulation of Ca^{2+} -ATPase, RMSD for the MD simulations of four ATP-bound proteins, performance and convergence of REMD simulation, and a comparison of PMF with X-ray structure. This material is available free of charge via the Internet at <http://pubs.acs.org>.

AUTHOR INFORMATION

Corresponding Author

*Tel.: +81-48-462-1407. Fax: +81-48-467-4532. E-mail: sugita@riken.jp.

Notes

The authors declare no competing financial interest.

ACKNOWLEDGMENTS

This research was supported in part by the RIKEN iTHES project and the Fund from the High Performance Computing Infrastructure (HPCI) Strategic Program of MEXT (to Y.S.). We also thank the RIKEN Integrated Cluster of Clusters (RICC) and MEXT SPIRE Supercomputational Life Science (SCLS) for providing computational resources.

■ ABBREVIATIONS

SERCA, sarcoplasmic reticulum Ca^{2+} -ATPase; ATP, adenosine triphosphate; ADP, adenosine diphosphate; MD, molecular dynamics; REMD, replica-exchange molecular dynamics; DOPC, dioleoylphosphatidylcholine; RMSD, root-mean-square deviation; RMSE, root-mean-square error; C27(ATP), CHARMM27 force-field parameters for polyphosphates; mod-C27(ATP), modified CHARMM27 force-field parameters for polyphosphates

■ REFERENCES

- (1) Møller, J. V.; Juul, B.; le Maire, M. Structural organization, ion transport, and energy transduction of P-type ATPases. *Biochim. Biophys. Acta* **1996**, *1286*, 1–51.
- (2) Albers, R. W. Biochemical Aspects of Active Transport. *Annu. Rev. Biochem.* **1967**, *36*, 727–756.
- (3) Post, R. L.; Hegyvary, C.; Kume, S. Activation by Adenosine Triphosphate in the Phosphorylation Kinetics of Sodium and Potassium Ion Transport Adenosine Triphosphatase. *J. Biol. Chem.* **1972**, *247*, 6530–6540.
- (4) Meis, L.; Vianna, A. L. Energy Interconversion by the Ca^{2+} Dependent ATPase of the Sarcoplasmic Reticulum. *Annu. Rev. Biochem.* **1979**, *48*, 275–292.
- (5) Toyoshima, C.; Mizutani, T. Crystal structure of the calcium pump with a bound ATP analogue. *Nature* **2004**, *430*, 529–535.
- (6) Sørensen, T. L.-M.; Møller, J. V.; Nissen, P. Phosphoryl transfer and calcium ion occlusion in the calcium pump. *Science* **2004**, *304*, 1672–1675.
- (7) Toyoshima, C.; Inesi, G. Structural basis of ion pumping by Ca^{2+} -ATPase of the sarcoplasmic reticulum. *Annu. Rev. Biochem.* **2004**, *73*, 269–292.
- (8) Inesi, G.; Lewis, D.; Ma, H.; Prasad, A.; Toyoshima, C. Concerted Conformational Effects of Ca^{2+} and ATP Are Required for Activation of Sequential Reactions in the Ca^{2+} ATPase (SERCA) Catalytic Cycle. *Biochemistry* **2006**, *45*, 13769–13778.
- (9) Toyoshima, C. How Ca^{2+} -ATPase pumps ions across the sarcoplasmic reticulum membrane. *Biochim. Biophys. Acta* **2009**, *1793*, 941–946.
- (10) Toyoshima, C. Structural aspects of ion pumping by Ca^{2+} -ATPase of sarcoplasmic reticulum. *Arch. Biochem. Biophys.* **2008**, *476*, 3–11.
- (11) Bublitz, M.; Poulsen, H.; Morth, J. P.; Nissen, P. In and out of the cation pumps: P-type ATPase structure revisited. *Curr. Opin. Struct. Biol.* **2010**, *20*, 431–439.
- (12) Bublitz, M.; Morth, J. P.; Nissen, P. P-type ATPases at a glance. *J. Cell Sci.* **2011**, *124*, 2515–2519.
- (13) Sugita, Y.; Ikeguchi, M.; Toyoshima, C. Relationship between Ca^{2+} -affinity and shielding of bulk water in the Ca^{2+} -pump from molecular dynamics simulations. *Proc. Natl. Acad. Sci. U. S. A* **2010**, *107*, 21465–21469.
- (14) Musgaard, M.; Thøgersen, L.; Schiøtt, B.; Tajkhorshid, E. Tracing cytoplasmic Ca^{2+} ion and water access points in the Ca^{2+} -ATPase. *Biophys. J.* **2012**, *102*, 268–277.
- (15) Sugita, Y.; Miyashita, N.; Ikeguchi, M.; Kidera, A.; Toyoshima, C. Protonation of the acidic residues in the transmembrane cation-binding sites of the Ca^{2+} pump. *J. Am. Chem. Soc.* **2005**, *127*, 6150–6151.
- (16) Musgaard, M.; Thøgersen, L.; Schiøtt, B. Protonation states of important acidic residues in the central Ca^{2+} ion binding sites of the Ca^{2+} -ATPase: a molecular modeling study. *Biochemistry* **2011**, *50*, 11109–11120.
- (17) Lervik, A.; Bresme, F.; Kjelstrup, S. Molecular dynamics simulations of the Ca^{2+} -pump: a structural analysis. *Phys. Chem. Chem. Phys.* **2012**, *14*, 3543–3553.
- (18) Espinoza-Fonseca, L. M.; Thomas, D. D. Atomic-level characterization of the activation mechanism of SERCA by calcium. *PLoS One* **2011**, *6*, e26936.
- (19) Nagarajan, A.; Andersen, J. P.; Woolf, T. B. Coarse-grained simulations of transitions in the E2-to-E1 conformations for Ca ATPase (SERCA) show entropy-enthalpy compensation. *J. Mol. Biol.* **2012**, *422*, 575–593.
- (20) Nagarajan, A.; Andersen, J. P.; Woolf, T. B. The role of domain: domain interactions versus domain: water interactions in the coarse-grained simulations of the E1P to E2P transitions in Ca-ATPase (SERCA). *Proteins* **2012**, *80*, 1929–1947.
- (21) Das, A.; Gur, M.; Cheng, M. H.; Jo, S.; Bahar, I.; Roux, B. Exploring the Conformational Transitions of Biomolecular Systems Using a Simple Two-State Anisotropic Network Model. *PLoS Comput. Biol.* **2014**, *10*, e1003521.
- (22) Li, G.; Cui, Q. A Coarse-Grained Normal Mode Approach for Macromolecules: An Efficient Implementation and Application to Ca^{2+} -ATPase. *Biophys. J.* **2002**, *83*, 2457–2474.
- (23) Reuter, N.; Hinsen, K.; Lacapère, J.-J. Transconformations of the SERCA1 Ca-ATPase: A Normal Mode Study. *Biophys. J.* **2003**, *85*, 2186–2197.
- (24) Li, G.; Cui, Q. Analysis of Functional Motions in Brownian Molecular Machines with an Efficient Block Normal Mode Approach: Myosin-II and Ca^{2+} -ATPase. *Biophys. J.* **2004**, *86*, 743–763.
- (25) Wriggers, W.; Schulten, K. Investigating a back door mechanism of actin phosphate release by steered molecular dynamics. *Proteins: Struct., Funct., Bioinf.* **1999**, *35*, 262–273.
- (26) Mesentean, S.; Koppole, S.; Smith, J. C.; Fischer, S. The Principal Motions Involved in the Coupling Mechanism of the Recovery Stroke of the Myosin Motor. *J. Mol. Biol.* **2007**, *367*, 591–602.
- (27) Splettstoesser, T.; Noé, F.; Oda, T.; Smith, J. C. Nucleotide-dependence of G-actin conformation from multiple molecular dynamics simulations and observation of a putatively polymerization-competent superclosed state. *Proteins: Struct., Funct., Bioinf.* **2009**, *76*, 353–364.
- (28) Shi, W.; Inamdar, M. V.; Sastry, A. M.; Lastoskie, C. M. Divalent Cation Adsorption on the Actin Monomer. *J. Phys. Chem. C* **2007**, *111*, 15642–15652.
- (29) Rennebaum, S.; Caflisch, A. Inhibition of interdomain motion in G-actin by the natural product latrunculin: A molecular dynamics study. *Proteins: Struct., Funct., Bioinf.* **2012**, *80*, 1998–2008.
- (30) Ng, Y.-W.; Raghunathan, D.; Chan, P. M.; Baskaran, Y.; Smith, D. J.; Lee, C.-H.; Verma, C.; Manser, E. Why an A-Loop Phospho-Mimetic Fails to Activate PAK1: Understanding an Inaccessible Kinase State by Molecular Dynamics Simulations. *Structure* **2010**, *18*, 879–890.
- (31) Jones, P. M.; George, A. M. Mechanism of ABC transporters: A molecular dynamics simulation of a well characterized nucleotide-binding subunit. *Proc. Natl. Acad. Sci. U. S. A* **2002**, *99*, 12639–12644.
- (32) Li, G.; Cui, Q. Mechanochemical Coupling in Myosin: A Theoretical Analysis with Molecular Dynamics and Combined QM/MM Reaction Path Calculations. *J. Phys. Chem. B* **2004**, *108*, 3342–3357.
- (33) Ito, Y.; Ikeguchi, M. Structural fluctuation and concerted motions in F_1 -ATPase: A molecular dynamics study. *J. Comput. Chem.* **2010**, *31*, 2175–2185.
- (34) Ito, Y.; Oroguchi, T.; Ikeguchi, M. Mechanism of the conformational change of the F_1 -ATPase β subunit revealed by free energy simulations. *J. Am. Chem. Soc.* **2011**, *133*, 3372–3380.
- (35) Ito, Y.; Yoshidome, T.; Matubayasi, N.; Kinoshita, M.; Ikeguchi, M. Molecular Dynamics Simulations of Yeast F_1 -ATPase before and after 16° Rotation of the γ Subunit. *J. Phys. Chem. B* **2013**, *117*, 3298–3307.
- (36) Yang, W.; Gao, Y. Q.; Cui, Q.; Ma, J.; Karplus, M. The missing link between thermodynamics and structure in F_1 -ATPase. *Proc. Natl. Acad. Sci. U. S. A.* **2003**, *100*, 874–879.
- (37) Gao, Y. Q.; Yang, W.; Karplus, M. A structure-based model for the synthesis and hydrolysis of ATP by F_1 -ATPase. *Cell* **2005**, *123*, 195–205.

- (38) Ma, J.; Flynn, T. C.; Cui, Q.; Leslie, A. G. W.; Walker, J. E.; Karplus, M. A Dynamic Analysis of the Rotation Mechanism for Conformational Change in F₁-ATPase. *Structure* **2002**, *10*, 921–931.
- (39) Yang, Y.; Yu, H.; Cui, Q. Extensive conformational transitions are required to turn on ATP hydrolysis in myosin. *J. Mol. Biol.* **2008**, *381*, 1407–1420.
- (40) Sugita, Y.; Okamoto, Y. Replica-exchange molecular dynamics method for protein folding. *Chem. Phys. Lett.* **1999**, *314*, 141–151.
- (41) Pavelites, J. J.; Gao, J.; Bash, P. A.; MacKerell, A. D. A molecular mechanics force field for NAD⁺ NADH, and the pyrophosphate groups of nucleotides. *J. Comput. Chem.* **1997**, *18*, 221–239.
- (42) Frisch, M. J.; Trucks, G. W.; Schlegel, H. B.; Scuseria, G. E.; Robb, M. A.; Cheeseman, J. R.; Scalmani, G.; Barone, V.; Mennucci, B.; Petersson, G. A.; Nakatsuji, H.; Caricato, M.; Li, X.; Hratchian, H. P.; Izmaylov, A. F.; Bloino, J.; Zheng, G.; Sonnenberg, J. L.; Hada, M.; Ehara, M.; Toyota, K.; Fukuda, R.; Hasegawa, J.; Ishida, M.; Nakajima, T.; Honda, Y.; Kitao, O.; Nakai, H.; Vreven, T.; Montgomery, J. A., Jr.; Peralta, J. E.; Ogliaro, F.; Bearpark, M.; Heyd, J. J.; Brothers, E.; Kudin, K. N.; Staroverov, V. N.; Kobayashi, R.; Normand, J.; Raghavachari, K.; Rendell, A.; Burant, J. C.; Iyengar, S. S.; Tomasi, J.; Cossi, M.; Rega, N.; Millam, N. J.; Klene, M.; Knox, J. E.; Cross, J. B.; Bakken, V.; Adamo, C.; Jaramillo, J.; Gomperts, R.; Stratmann, R. E.; Yazyev, O.; Austin, A. J.; Cammi, R.; Pomelli, C.; Ochterski, J. W.; Martin, R. L.; Morokuma, K.; Zakrzewski, V. G.; Voth, G. A.; Salvador, P.; Dannenberg, J. J.; Dapprich, S.; Daniels, A. D.; Farkas, Ö.; Foresman, J. B.; Ortiz, J. V.; Cioslowski, J.; Fox, D. J. *Gaussian 09*, Revision A.1; Gaussian, Inc.: Wallingford, CT, 2009.
- (43) Guvench, O.; MacKerell, A. D., Jr. Automated conformational energy fitting for force-field development. *J. Mol. Model.* **2008**, *14*, 667–679.
- (44) Meagher, K. L.; Redman, L. T.; Carlson, H. A. Development of polyphosphate parameters for use with the AMBER force field. *J. Comput. Chem.* **2003**, *24*, 1016–1025.
- (45) Foloppe, N.; MacKerell, J. All-atom empirical force field for nucleic acids: I. Parameter optimization based on small molecule and condensed phase macromolecular target data. *J. Comput. Chem.* **2000**, *21*, 86–104.
- (46) MacKerell, A. D.; Banavali, N. K. All-atom empirical force field for nucleic acids: II. Application to molecular dynamics simulations of DNA and RNA in solution. *J. Comput. Chem.* **2000**, *21*, 105–120.
- (47) Toyoshima, C.; Nakasako, M.; Nomura, H.; Ogawa, H. Crystal structure of the calcium pump of sarcoplasmic reticulum at 2.6 Å resolution. *Nature* **2000**, *405*, 647–655.
- (48) Humphrey, W.; Dalke, A.; Schulten, K. VMD: Visual molecular dynamics. *J. Mol. Graphics* **1996**, *14*, 33–38.
- (49) Gumbart, J.; Trabuco, L. G.; Schreiner, E.; Villa, E.; Schulten, K. Regulation of the protein-conducting channel by a bound ribosome. *Structure* **2009**, *17*, 1453–1464.
- (50) Jo, S.; Kim, T.; Im, W. Automated Builder and Database of Protein/Membrane Complexes for Molecular Dynamics Simulations. *PLoS One* **2007**, *2*, e880.
- (51) Jo, S.; Kim, T.; Iyer, V. G.; Im, W. CHARMM-GUI: A web-based graphical user interface for CHARMM. *J. Comput. Chem.* **2008**, *29*, 1859–1865.
- (52) Jo, S.; Lim, J. B.; Klauda, J. B.; Im, W. CHARMM-GUI Membrane Builder for Mixed Bilayers and Its Application to Yeast Membranes. *Biophys. J.* **2009**, *97*, 50–58.
- (53) MacKerell, A. D.; Feig, M.; Brooks, C. L., III. Extending the treatment of backbone energetics in protein force fields: limitations of gas-phase quantum mechanics in reproducing protein conformational distributions in molecular dynamics simulations. *J. Comput. Chem.* **2004**, *25*, 1400–1415.
- (54) MacKerell, A. D.; Bashford, D.; Dunbrack, R. L.; Evanseck, J. D.; Field, M. J.; Fischer, S.; Gao, J.; Guo, H.; Ha, S.; Joseph-McCarthy, D.; Kuchnir, L.; Kuczera, K.; Lau, F. T. K.; Mattos, C.; Michnick, S.; Ngo, T.; Nguyen, D. T.; Prodhom, B.; Reiher, W. E.; Roux, B.; Schlenkrich, M.; Smith, J. C.; Stote, R.; Straub, J.; Watanabe, M.; Wiórkiewicz-Kuczera, J.; Yin, D.; Karplus, M. All-Atom Empirical Potential for Molecular Modeling and Dynamics Studies of Proteins. *J. Phys. Chem. B* **1998**, *102*, 3586–3616.
- (55) Klauda, J. B.; Venable, R. M.; Freites, J. A.; O'Connor, J. W.; Tobias, D. J.; Mondragon-Ramirez, C.; Vorobyov, I.; MacKerell, A. D., Jr.; Pastor, R. W. Update of the CHARMM all-atom additive force field for lipids: validation on six lipid types. *J. Phys. Chem. B* **2010**, *114*, 7830–7843.
- (56) Jorgensen, W. L.; Chandrasekhar, J.; Madura, J. D.; Impey, R. W.; Klein, M. L. Comparison of simple potential functions for simulating liquid water. *J. Chem. Phys.* **1983**, *79*, 926–935.
- (57) Allnér, O.; Nilsson, L.; Villa, A. Magnesium Ion–Water Coordination and Exchange in Biomolecular Simulations. *J. Chem. Theory Comput.* **2012**, *8*, 1493–1502.
- (58) Åqvist, J. Ion-water interaction potentials derived from free energy perturbation simulations. *J. Phys. Chem.* **1990**, *94*, 8021–8024.
- (59) Ryckaert, J.; Ciccotti, G.; Berendsen, H. Numerical integration of the cartesian equations of motion of a system with constraints: molecular dynamics of *n*-alkanes. *J. Comput. Phys.* **1977**, *23*, 327–341.
- (60) Miyamoto, S.; Kollman, P. A. Settle: An analytical version of the SHAKE and RATTLE algorithm for rigid water models. *J. Comput. Chem.* **1992**, *13*, 952–962.
- (61) Essmann, U.; Perera, L.; Berkowitz, M. L.; Darden, T.; Lee, H.; Pedersen, L. G. A smooth particle mesh Ewald method. *J. Chem. Phys.* **1995**, *103*, 8577–8593.
- (62) Feller, S. E.; Zhang, Y.; Pastor, R. W.; Brooks, B. R. Constant pressure molecular dynamics simulation: The Langevin piston method. *J. Chem. Phys.* **1995**, *103*, 4613–4621.
- (63) Hoover, W. Canonical dynamics: Equilibrium phase-space distributions. *Phys. Rev. A* **1985**, *31*, 1695–1697.
- (64) Phillips, J. C.; Braun, R.; Wang, W.; Gumbart, J.; Tajkhorshid, E.; Villa, E.; Chipot, C.; Skeel, R. D.; Kalé, L.; Schulten, K. Scalable molecular dynamics with NAMD. *J. Comput. Chem.* **2005**, *26*, 1781–1802.
- (65) Miyashita, N.; Re, S.; Sugita, Y. REIN: Replica-Exchange INterface for Simulating Protein Dynamics and Function. *Int. J. Quantum Chem.* **2014**, in press.
- (66) Patriksson, A.; van der Spoel, D. A temperature predictor for parallel tempering simulations. *Phys. Chem. Chem. Phys.* **2008**, *10*, 2073–2077.
- (67) Daiho, T.; Yamasaki, K.; Danko, S.; Suzuki, H. Critical role of Glu⁴⁰-Ser⁴⁸ loop linking actuator domain and first transmembrane helix of Ca²⁺-ATPase in Ca²⁺ deocclusion and release from ADP-insensitive phosphoenzyme. *J. Biol. Chem.* **2007**, *282*, 34429–34447.
- (68) Hilge, M.; Siegal, G.; Vuister, G. W.; Güntert, P.; Gloor, S. M.; Abrahams, J. P. ATP-induced conformational changes of the nucleotide-binding domain of Na⁺, K⁺-ATPase. *Nat. Struct. Mol. Biol.* **2003**, *10*, 468–474.
- (69) McIntosh, D. B.; Woolley, D. G.; Vilnsen, B.; Andersen, J. P. Mutagenesis of Segment ⁴⁸⁷Phe-Ser-Arg-Asp-Arg-Lys⁴⁹² of Sarcoplasmic Reticulum Ca²⁺-ATPase Produces Pumps Defective in ATP Binding. *J. Biol. Chem.* **1996**, *271*, 25778–25789.
- (70) Toyoshima, C.; Yonekura, S.; Tsueda, J.; Iwasawa, S. Trinitrophenyl derivatives bind differently from parent adenine nucleotides to Ca²⁺-ATPase in the absence of Ca²⁺. *Proc. Natl. Acad. Sci. U. S. A* **2011**, *108*, 1833–1838.
- (71) Sacchetto, R.; Bertipaglia, I.; Giannetti, S.; Cendron, L.; Mascarello, F.; Damiani, E.; Carafoli, E.; Zanotti, G. Crystal structure of sarcoplasmic reticulum Ca²⁺-ATPase (SERCA) from bovine muscle. *J. Struct. Biol.* **2012**, *178*, 38–44.
- (72) Bublitz, M.; Musgaard, M.; Poulsen, H.; Thøgersen, L.; Olesen, C.; Schiott, B.; Morth, J. P.; Muller, J. V.; Nissen, P. Ion pathways in the sarcoplasmic reticulum Ca²⁺-ATPase. *J. Biol. Chem.* **2013**, *288*, 10759–10765.
- (73) Clarke, D. M.; Loo, T. W.; MacLennan, D. H. Functional consequences of alterations to amino acids located in the nucleotide binding domain of the Ca²⁺-ATPase of sarcoplasmic reticulum. *J. Biol. Chem.* **1990**, *265*, 22223–22227.
- (74) Maruyama, K.; Clarke, D. M.; Fujii, J.; Inesi, G.; Loo, T. W.; MacLennan, D. H. Functional consequences of alterations to amino

- acids located in the catalytic center (isoleucine 348 to threonine 357) and nucleotide-binding domain of the Ca^{2+} -ATPase of sarcoplasmic reticulum. *J. Biol. Chem.* **1989**, *264*, 13038–13042.
- (75) McIntosh, D. B.; Woolley, D. G.; MacLennan, D. H.; Vilsen, B.; Andersen, J. P. Interaction of Nucleotides with Asp³⁵¹ and the Conserved Phosphorylation Loop of Sarcoplasmic Reticulum Ca^{2+} -ATPase. *J. Biol. Chem.* **1999**, *274*, 25227–25236.
- (76) Ma, H.; Inesi, G.; Toyoshima, C. Substrate-induced Conformational Fit and Headpiece Closure in the Ca^{2+} ATPase (SERCA). *J. Biol. Chem.* **2003**, *278*, 28938–28943.
- (77) Clausen, J. D.; McIntosh, D. B.; Vilsen, B.; Woolley, D. G.; Andersen, J. P. Importance of Conserved N-domain Residues Thr⁴⁴¹, Glu⁴⁴², Lys⁵¹⁵, Arg⁵⁶⁰, and Leu⁵⁶² of Sarcoplasmic Reticulum Ca^{2+} -ATPase for MgATP Binding and Subsequent Catalytic Steps: PLASTICITY OF THE NUCLEOTIDE-BINDING SITE. *J. Biol. Chem.* **2003**, *278*, 20245–20258.
- (78) Jacobsen, M. D.; Pedersen, P. A.; Jorgensen, P. L. Importance of Na,K-ATPase Residue α 1-Arg⁵⁴⁴ in the Segment Arg⁵⁴⁴–Asp⁵⁶⁷ for High-Affinity Binding of ATP, ADP, or MgATP. *Biochemistry* **2002**, *41*, 1451–1456.
- (79) Beglov, D.; Roux, B. Finite representation of an infinite bulk system: solvent boundary potential for computer simulations. *J. Chem. Phys.* **1994**, *100*, 9050–9063.
- (80) Babu, C. S.; Lim, C. Theory of ionic hydration: insights from molecular dynamics simulations and experiment. *J. Phys. Chem. B* **1999**, *103*, 7958–7968.
- (81) Sakharov, D. V.; Lim, C. Zn protein simulations including charge transfer and local polarization effects. *J. Am. Chem. Soc.* **2005**, *127*, 4921–4929.
- (82) Babu, C. S.; Lim, C. Empirical force fields for biologically active divalent metal cations in water. *J. Phys. Chem. A* **2006**, *110*, 691–699.
- (83) Jiao, D.; King, C.; Grossfield, A.; Darden, T. A.; Ren, P. Simulation of Ca^{2+} and Mg^{2+} solvation using polarizable atomic multipole potential. *J. Phys. Chem. B* **2006**, *110*, 18553–18559.
- (84) Oelschlaeger, P.; Klahn, M.; Beard, W. A.; Wilson, S. H.; Warshel, A. Magnesium-cationic dummy atom molecules enhance representation of DNA polymerase β in molecular dynamics simulations: Improved accuracy in studies of structural features and mutational effects. *J. Mol. Biol.* **2007**, *366*, 687–701.
- (85) Neves, R. P. P.; Sousa, S. F.; Fernandes, P. A.; Ramos, M. J. Parameters for molecular dynamics simulations of manganese-containing metalloproteins. *J. Chem. Theory Comput.* **2013**, *9*, 2718–2732.
- (86) Li, P.; Roberts, B. P.; Chakravorty, D. K.; Merz, K. M., Jr. Rational Design of Particle Mesh Ewald Compatible Lennard-Jones Parameters for +2 Metal Cations in Explicit Solvent. *J. Chem. Theory Comput.* **2013**, *9*, 2733–2748.
- (87) Li, P.; Merz, K. M., Jr. Taking into Account the Ion-induced Dipole Interaction in the Nonbonded Model of Ions. *J. Chem. Theory Comput.* **2014**, *10*, 289–297.
- (88) Kuzcera, K.; Wiorkiewicz-Kuzcera, J.; Karplus, M. *The MOLVIB Module of CHARMM*, version c36b2; Dept. of Chemistry, Harvard University: Cambridge, MA, 1991.